Nanoscale Res Lett (2010) 5:149–157
DOI 10.1007/s11671-009-9457-9

NANO EXPRESS

Effect of Surfactants on the Structure and Morphology of Magnesium Borate Hydroxide Nanowhiskers Synthesized by Hydrothermal Route

Latha Kumari · W. Z. Li · Shrinivas Kulkarni · K. H. Wu · Wei Chen · Chunlei Wang · Charles H. Vannoy · Roger M. Leblanc

Received: 5 August 2009 / Accepted: 26 September 2009 / Published online: 13 October 2009

Abstract Magnesium borate hydroxide (MBH) nanowhiskers were synthesized using a one step hydrothermal process with different surfactants. The effect surfactants have on the structure and morphology of the MBH nanowhiskers has been investigated. The X-ray diffraction profile confirms that the as-synthesized material is of single phase, monoclinic $MgBO_2(OH)$. The variations in the size and shape of the different MBH nanowhiskers have been discussed based on the surface morphology analysis. The annealing of MBH nanowhiskers at 500 °C for 4 h has significant effect on the crystal structure and surface morphology. The UV–vis absorption spectra of the MBH nanowhiskers synthesized with and without surfactants show enhanced absorption in the low-wavelength region, and their optical band gaps were estimated from the optical band edge plots. The photoluminescence spectra of the MBH nanowhiskers produced with and without surfactants show broad emission band with the peak maximum at around 400 nm, which confirms the dominant contribution from the surface defect states.

L. Kumari · W. Z. Li (✉)
Department of Physics, Florida International University, Miami, FL 33199, USA
e-mail: Wenzhi.Li@fiu.edu

S. Kulkarni · K. H. Wu · W. Chen · C. Wang
Department of Mechanical and Materials Engineering, Florida International University, Miami, FL 33174, USA

C. H. Vannoy · R. M. Leblanc
Department of Chemistry, University of Miami, Coral Gables, FL 33124, USA

Keywords Magnesium borate hydroxide · Nanowhiskers · Hydrothermal synthesis · Surface morphology · X-ray diffraction

Introduction

Nanostructured materials have received great interest due to their fascinating physical, optical, electrical, and thermoelectric properties as well as their potential applications in nanodevices [1–4]. Metal borates are considered among the most important of these materials because of their unique properties, such as their light weight, high strength, high heat-resistance, corrosion-resistance, and high coefficient of elasticity, etc. Hence, the nanoscale metal borates are ideal for exploring their potential applications in the fields of nanocomposites, nanomechanics, and nano-electronics. Among the various metal borates, aluminum borate is perhaps the best known ceramic material with chemical stability, enhanced mechanical properties and potential applications in high-temperature composites [5]. Magnesium borate is another remarkable ceramic material that shows excellent mechanical and thermal properties.

Magnesium borate hydroxide ($MgBO_2(OH)$), also known as the Szaibelyite, is a widely available translucent mineral in nature and is used as the main source of boron in industry [6, 7]. The Szaibelyite is also an important source of anhydrous magnesium borate [8]. Magnesium borate can be used as thermo-luminescent phosphor [9], antiwear and friction reducing additive [10], ferro-elastic material [11], which is a candidate for tunable laser applications [12], and can be used as a luminescent material for fluorescent discharge lamps, cathode ray tube screens, and X-ray screens [13]. Recently variety of magnesium borate nanostructures such as nanorods [14], nanowires [15, 16], nanobelts [17],

nanoparticles [10] and nanotubes [18] have been fabricated by different synthesis techniques including thermal evaporation, chemical vapor deposition, ethanol supercritical fluid drying technique, and thermal evaporation in IR-irradiation heating furnace [10, 14–18]. However, in all these reported routes, the synthesis was performed at high temperatures (750–1,100 °C).

The synthesis of nanoparticles with controlled size and shape results in new electronic and optical properties, which is suitable for many electronic and optoelectronic applications [19]. The use of surfactants as stabilizers has advantages with the fact that these surface-active chemicals possess sufficient strength to effectively control the particle size growth. The surfactants support to have particles with "monodisperse" size distribution and increased aspect ratio, and they also effectively prevent the particles from agglomeration [20–23]. Over the decades, the hydrothermal process has proved to be one of the most successful methods for synthesizing low dimensional materials. However, there exist very few reports on the synthesis of nanostructured $MgBO_2(OH)$ using the hydrothermal method [8, 24–26]. In addition, the conversion of magnesium borate hydroxide to anhydrous magnesium borate is rarely reported [7, 21]. Zhu et al. [8, 24, 25] reported the hydrothermal synthesis of $MgBO_2(OH)$ nanowhiskers using $MgCl_2$, H_3BO_3 and NaOH as the starting materials with molar ratio of Mg:B:Na as 2:3:4 at 240 °C for 18 h. Zhu et al. [25] also investigated the effect of the dropping rate of NaOH into the precursor solution, droplet size, and amount of the NaOH solution and the hydrothermal reaction time on the hydrothermal formation of the $MgBO_2(OH)$ nanowhiskers with other synthesis parameters kept constant. The morphology preservation and crystallinity improvement in the thermal conversion of the hydrothermal synthesized $MgBO_2(OH)$ nanowhiskers to $Mg_2B_2O_5$ nanowhiskers was investigated in the temperature range of 650–700 °C and was kept under isothermal condition for 2.0–4.0 h [8]. Xu et al. [27] demonstrated the growth of magnesium borate ($Mg_2B_2O_5$) nanorods at 400 °C (supercritical condition) by solvothermal route and explained that the temperature of 200 °C was not sufficient for synthesizing the well-defined nanostructures. In addition, the synthesis of the magnesium borate nanorods needs the assistance of surfactants/capping agents. In their work, the $MgBO_2(OH)$ columnar-like particles were synthesized at 320 °C with ethanol and water as solvents. In the present work, the MBH nanowhiskers with regular shape and size were successfully synthesized at a reaction temperature of 200 °C (H_2O as solvent) without using any surfactants/capping agents. Additionally, the effect of surfactants on the structure and surface morphology of the MBH nanomaterials is studied. Optical properties including UV–vis absorption and photoluminescence (PL) of the MBH nanowhiskers are also investigated.

Experiments

All chemicals used for the synthesis of magnesium borate hydroxide nanostructures were analytical grade (Fisher Scientific) and used without further purification. In a typical synthesis, 3.846 g of magnesium nitrate hexahydrate ($MgNO_3{\cdot}6H_2O$) and 0.568 g of sodium borohydrate ($NaBH_4$) were separately mixed in 10 mL distilled water. Then the two solutions were put together and placed in ultrasonicator (Branson, Model 2510, 40 kHz) for about 30 min to get homogeneous and clear solution. The solution was put into a Teflon liner (30 mL capacity) up to 80% of the total volume. The Teflon lined autoclave was sealed and placed in a furnace and maintained at 200 °C for 24 h (in air). After the completion of the hydrothermal reaction, the autoclave was cooled down to room temperature naturally. The precipitate was filtered and washed repeatedly with distilled water and ethanol (100% Reagent alcohol, Fisher Scientific) and was later dried at 100 °C for 4 h. The procured powders were used further for various characterizations. The above synthesis procedure was repeated for 1.5 M $MgNO_3{\cdot}6H_2O$ and 1.5 M $NaBH_4$ with the addition of 0.184 g (0.1 M) Cetyl trimethylammonium bromide (CTAB), 0.144 g (0.1 M) sodium dodecyl sulfate (SDS) and 2 mL Triton X-100, respectively, at 200 °C for 24 h. The surfactants CTAB, SDS and Triton are cationic, anionic and non-ionic, respectively. The magnesium borate hydroxide nanowhiskers synthesized with and without surfactant were annealed at 500 °C for 4 h in air. The heating rate of 6 °C/min and cooling rate of 0.5 °C/min were maintained constant for each of the nanowhiskers synthesis. The magnesium borate hydroxide nanowhiskers fabricated without surfactant and with CTAB, SDS and Triton are termed as MBH-NON, MBH-CTAB, MBH-SDS and MBH-Triton, respectively. To investigate the effect of synthesis process on the nanostructure formation, the $MgBO_2(OH)$ samples were also produced by heating the starting materials in open beaker at 150 °C for 6 h in air.

Surface morphology analysis of the MBH nanostructures was performed by a field emission scanning electron microscope (SEM, JEOL JSM-6330F, 15 kV). X-ray diffraction (XRD) measurements were carried out using Siemens D5000 diffractometer equipped with Cu anode operated at 40 kV and 40 mA. The XRD patterns were collected with step size of 0.01° and a scan rate of 1 s/step. UV–vis spectra were obtained from Perkin-Elmer Lambda 900 UV/Vis/NIR spectrometer, and the PL spectra were recorded from Horiba Jobin-Yvon FluoroLog FL3-22 spectrofluorometer. For the spectroscopic analysis, magnesium borate hydroxide powders were added to NaOH solution for a better dispersion, and the solution was taken into a quartz cell (1 cm optical path length) at room temperature.

Results and Discussion

X-ray Diffraction Analysis

X-ray diffraction analysis was carried out to investigate the crystalline phase of the as-synthesized materials. Figure 1 presents the XRD patterns of the nanowhiskers synthesized with and without surfactants. The XRD profiles (Fig. 1) for the MBH-NON, MBH-CTAB, MBH-SDS and MBH-Triton samples show that the as-prepared material is of single phase and high purity. All the diffraction peaks indicated by '*' can be indexed as the pure monoclinic phase of $MgBO_2(OH)$ with lattice constants of $a = 12.614$ Å, $b = 10.418$ Å, $c = 3.144$ Å, $\beta = 95.88°$ (JCPDS # 39-1370) [24, 26]. The broad background and the wide peaks observed for the XRD profiles (Fig. 1) indicate either that the crystallites of MBH are very small or the as-synthesized material is amorphous in nature [10]. XRD profiles show that the nanowhiskers synthesized without surfactant (MBH-NON) show sharp diffraction features when compared to that of the samples fabricated with surfactants (MBH-CTAB, MBH-SDS and MBH-Triton). The low angle peaks corresponding to (200) and (020) lattice planes show up as almost negligible features in the MBH-NON sample, whereas these peaks are prominent in MBH-CTAB, MBH-SDS and MBH-Triton samples. Also, a broad amorphous background between 10 and 25° is missing for the MBH-NON sample. From the XRD analysis, it can be concluded that the addition of surfactants results in a reduced intensity of the diffraction peaks for the as-synthesized MBH samples, but still maintains the crystalline phase of the material. However, the increase or decrease in the peak intensity depends on the lattice orientation or rearrangement. Surfactants typically play crucial roles in the particle size and size distribution. The addition of surfactant as capping agent/structure directing agent in the synthesis produces monodispersed and small size nanoparticles. The nanoparticles with smaller size diffract X-rays weakly and also give rise to amorphous background as observed for the XRD patterns (Fig. 1) of MBH samples synthesized with the addition of surfactants [28].

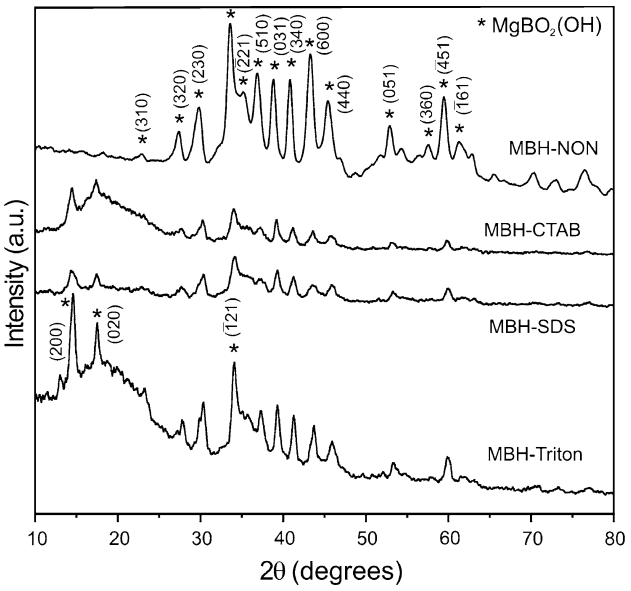

Fig. 1 XRD patterns of the as-synthesized magnesium borate hydroxide nanowhiskers formed with different surfactants and without surfactant

Surface Morphology Analysis

Figure 2 shows the SEM images of the magnesium borate hydroxide (MBH-NON) nanowhiskers synthesized without surfactant. The large-scale view of the MBH-NON sample in Fig. 2a confirms the uniform growth of the nanowhiskers. Figure 2b is the high-magnification image showing the nanowhiskers with almost uniform shape, width and length. Each of the nanowhiskers is around 45 nm wide and 450 nm long. Previous work by Zhu et al. [7, 18]

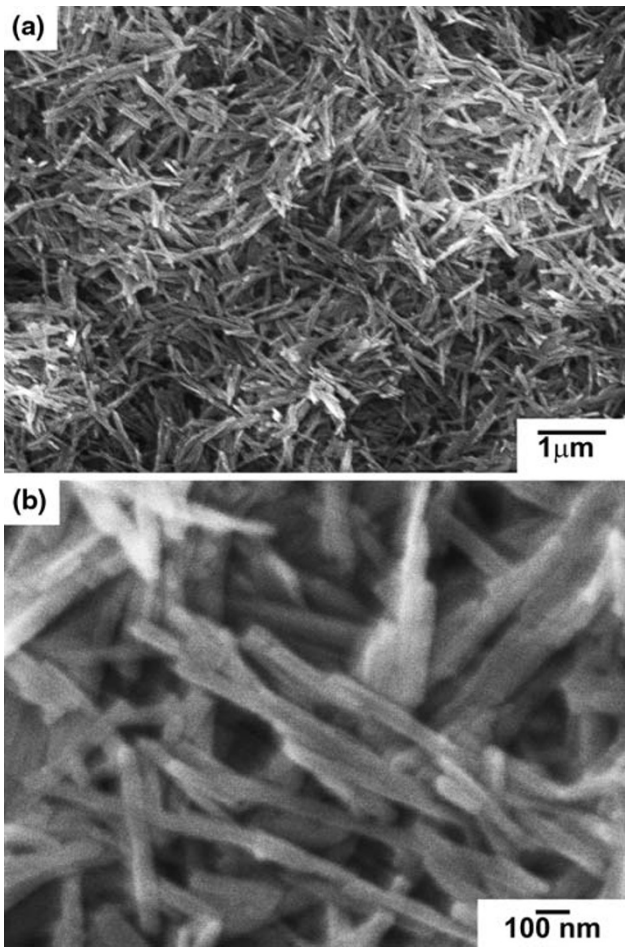

Fig. 2 **a** Low- and **b** high-magnification SEM images of magnesium borate hydroxide nanowhiskers fabricated without surfactant

reported the hydrothermal synthesis of nanowhiskers of variable length and width at 240 °C for 18 h. However, the synthesis procedure was different from the present work. To study the effect of surfactants on the surface morphology of the nanostructure, the MBH materials were also synthesized in the presence of surfactants. The surface morphology of MBH nanowhiskers fabricated with surfactants is as shown in Fig. 3. Figure 3a represents the high-magnification SEM image of MBH nanostructures produced with CTAB (MBH-CTAB). The MBH-CTAB sample shows nanowhiskers of length 300–650 nm and width 20–45 nm. The formation of MBH nanowhiskers with SDS (MBH-SDS) is presented by high-magnification SEM image in Fig. 3b. The MBH-SDS nanowhiskers are 300–350 nm long and 30 nm wide. The large-scale view of the MBH nanowhiskers fabricated with Triton as surfactant/capping agent (MBH-Triton) is shown in Fig. 3c, which indicates the formation of spherical clusters made up of fibrous nanowhiskers. The closer view (Fig. 3d) of these microspheres shows the cage-like structure formed with nanowhiskers, which have length of 500 nm to 1 μm and width of 20–40 nm. From the SEM analysis, it can be concluded that MBH nanowhiskers formed with the addition of surfactants are longer and thinner than the nanowhiskers synthesized without a surfactant, except for the MBH-SDS sample which has shorter nanowhiskers. The addition of surfactants induces the formation of nanowhiskers with reduced size and uneven shapes. The surfactants of various ionic phases (anionic, cationic and non-ionic) have been extensively used in the synthesis of nanostructures with controlled size, shape and aspect ratio [29–31]. In general, surfactants are considered as templates, structure directing agents or capping agents. Each of the different surfactants is found to have specific mechanism involved in the synthesis of nanostructures. During the synthesis process, the surfactants adsorb to the growing crystal, and depending upon the precursor concentrations and surfactant properties, it can moderate the growth rate of crystal faces, which thereby helps in the size and shape control [29–32].

Figure 4 is the low-magnification TEM image of MBH nanowhiskers synthesized without surfactant (MBH-NON). The inset of Fig. 4 is a closer view of the nanowhisker deformed in the presence of electron beam, which is confirmed by the random bulging and smearing of the nanowhisker surface. The deformation of the nanowhiskers in the presence of electron beam reveals the amorphous nature of the as-synthesized MBH-NON sample, which is also supported by the XRD analysis. From the TEM analysis, it can be concluded that the as-synthesized MBH nanowhiskers does not have hollow nature, but the close view of the high-magnification image in the inset of Fig. 4 reveals the porous structure. Previous works [24, 25] by Zhu et al. reported the better crystallinity of the MBH nanowhiskers

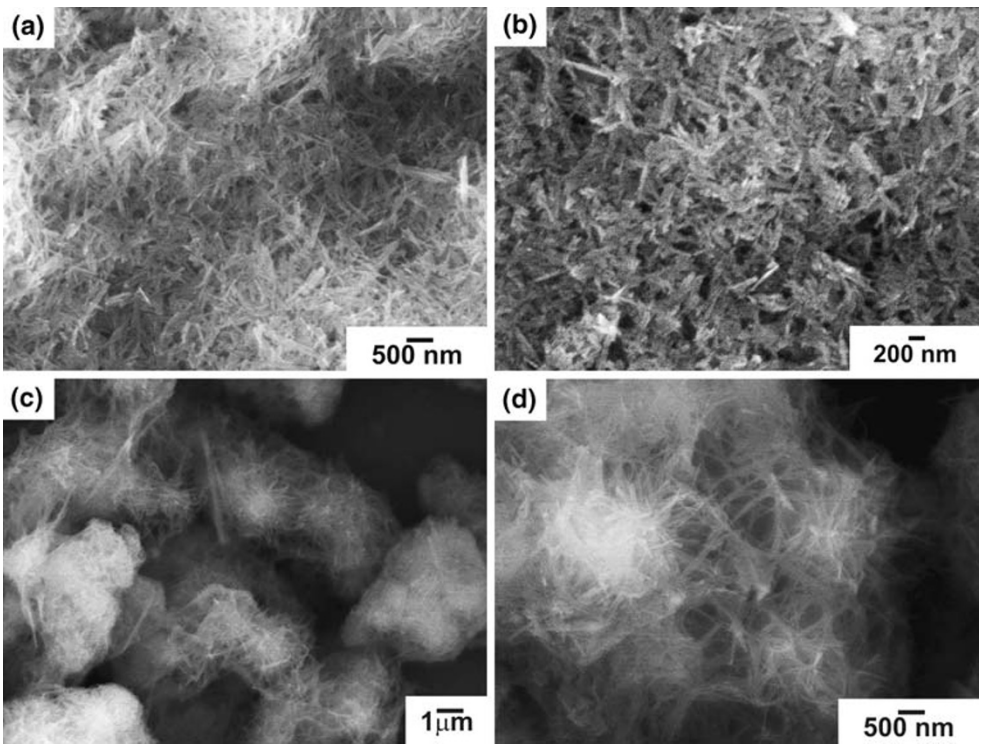

Fig. 3 SEM images of magnesium borate hydroxide nanowhiskers synthesized with **a** CTAB, **b** SDS, and **c**, **d** Triton at low and high magnification, respectively

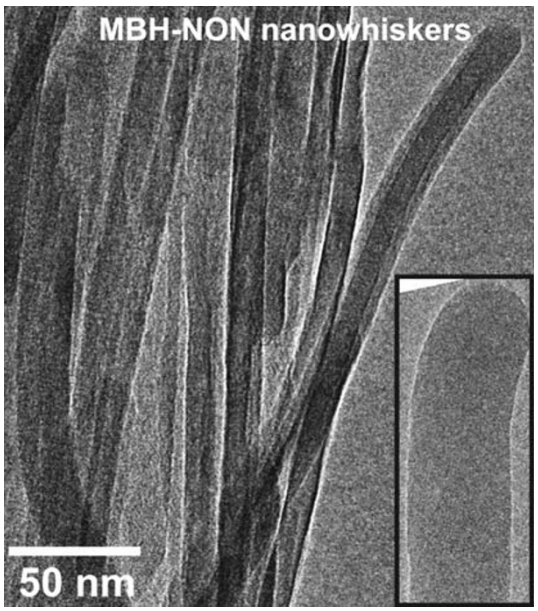

Fig. 4 TEM image of MBH-NON nanowhiskers. *Inset* is the high-magnification image of single nanowhisker

than the present work; however, the synthesis mechanism in their work was quite different from our work. Besides the study of the synthesis mechanism in our work, the thermal annealing effect on the surface morphology and crystal structure of the MBH nanowhiskers synthesized with and without surfactants is also studied.

Further, to understand the effect of sample processing conditions on the morphology, we performed the sample synthesis in open air instead of in an autoclave, where the precipitate of the starting materials was heated in open beaker at 150 °C for 6 h. Figure 5 shows the low and high-magnification image of the urchin-like nanowhiskers formed at 150 °C with addition of Triton. The close view of the urchin-like spherical clusters in the high-magnification image (Fig. 5b) reveals that each of the spherical clusters consist of tiny nanowhiskers. The open air processing of MBH nanowhiskers with the addition of Triton as surfactant has significant influence on the surface morphology. The hydrothermal synthesis at 200 °C for 24 h produced spherical clusters made up of fibrous nanowhiskers with length as long as 1 μm, whereas the synthesis at 150 °C for 6 h in air formed urchin-like spherical clusters with <100 nm long tiny nanowhiskers.

Effect of Annealing on the Crystal Structure and Surface Morphology

To understand the effect of annealing on the structure and surface morphology of the magnesium borate hydroxide nanostructures, the as-prepared MBH samples were annealed at 500 °C for 4 h with heating rate of about

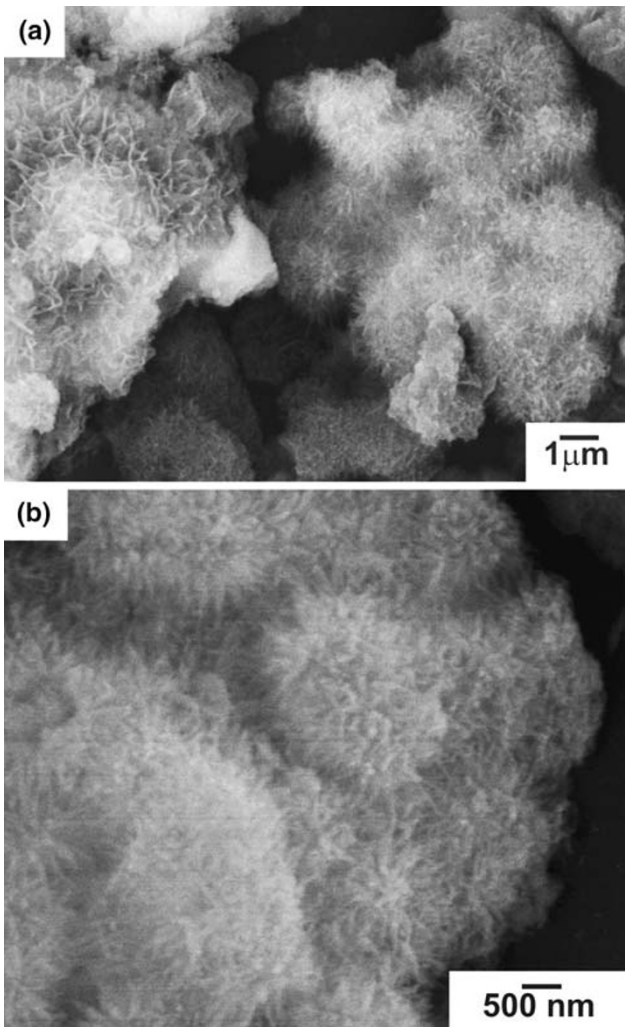

Fig. 5 Surface morphology of magnesium borate hydroxide urchin-like nanostructures fabricated at 150 °C for 6 h in open beaker at **a** low- and **b** high- magnification

8 °C/min. Figure 6 shows the XRD profiles for annealed MBH nanowhiskers synthesized with and without surfactants. All the diffraction peaks indicated by '*' can be indexed as the pure monoclinic phase of $MgBO_2(OH)$. Even though the XRD profile of the annealed MBH-NON sample does not reveal any crystalline phase change, it does show some structural changes in comparison with the as-prepared MBH-NON nanowhiskers (Fig. 1). In contrast with the XRD profile for as-prepared MBH-NON nanowhiskers in Fig. 1, the XRD pattern for the annealed MBH-NON nanowhiskers in Fig. 6 shows the obvious low angle peaks corresponding to (200) and (020) lattice planes of monoclinic $MgBO_2(OH)$, and the peak representing (−211) plane becomes more prominent. The increased peak intensity of the annealed MBH-NON nanowhiskers can be attributed to the change in lattice orientation [33]. XRD patterns of annealed MBH nanowhiskers synthesized with surfactants show broad amorphous-like feature

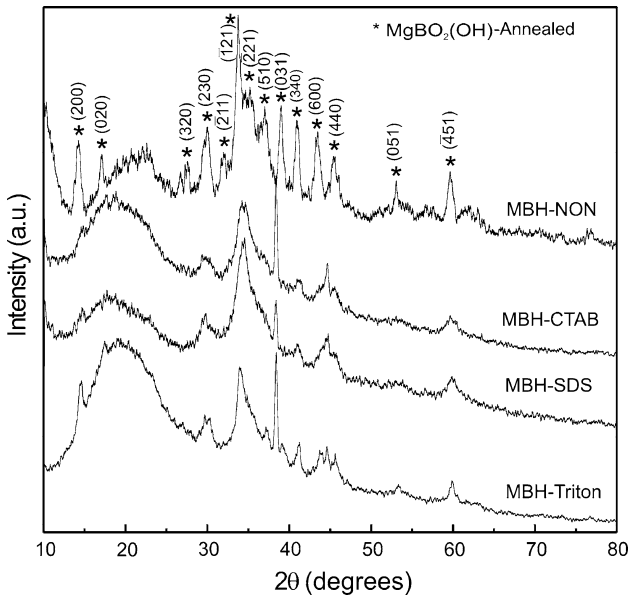

Fig. 6 XRD patterns of annealed MBH nanowhiskers synthesized with and without surfactants

between 10 and 30° and also indicate broader peaks with reduced intensity when compared with that of the un-annealed samples, revealing the reduced crystallinity. Previous report by Zhu et al. [8] also reported the appearance of poor crystallinity in the MBH nanowhiskers annealed at 500 °C for 2 h. Moreover, they also studied the annealing effect on MBH nanowhiskers at different annealing temperatures, duration and heating rate. In the present work, we have limited our studies to annealing at 500 °C only. The diffraction peaks for the annealed MBH nanowhiskers synthesized with surfactants show peak shift toward lower angles with respect to the MBH-NON nanowhiskers. The peak shift and peak broadening can be attributed to the internal strain in the crystal structure due to the stacking faults, grain boundaries and small crystallites, respectively arising from the polycrystalline nature and surface structure of the nanoparticles induced by thermal annealing [33].

Figure 7 shows the high-magnification SEM images of the annealed MBH nanowhiskers synthesized with and without surfactants. From the SEM image in Fig. 7a, it is evident that the nanowhiskers in the annealed MBH-NON sample show increased aspect ratio and slightly irregular shape when compared with that of the as-synthesized MBH-NON nanowhiskers (Fig. 2b). The nanowhiskers in the annealed MBH sample have a length of about 500 nm and widths of 10–40 nm. Figure 7b presents the high-magnification SEM image of the annealed MBH-CTAB nanowhiskers. The nanowhiskers show elongated fibrous-like structures with widths of 30–50 nm and lengths of 1–2 μm, which is much higher than the as-prepared nanowhiskers. The annealed MBH-SDS sample (Fig. 7c) also shows elongated fiber-like nanowhiskers that are 40–60 nm wide and 1–2 μm long. The high-magnification SEM image in Fig. 7d for MBH-Triton sample shows nanowhiskers with reduced width, but almost same length as

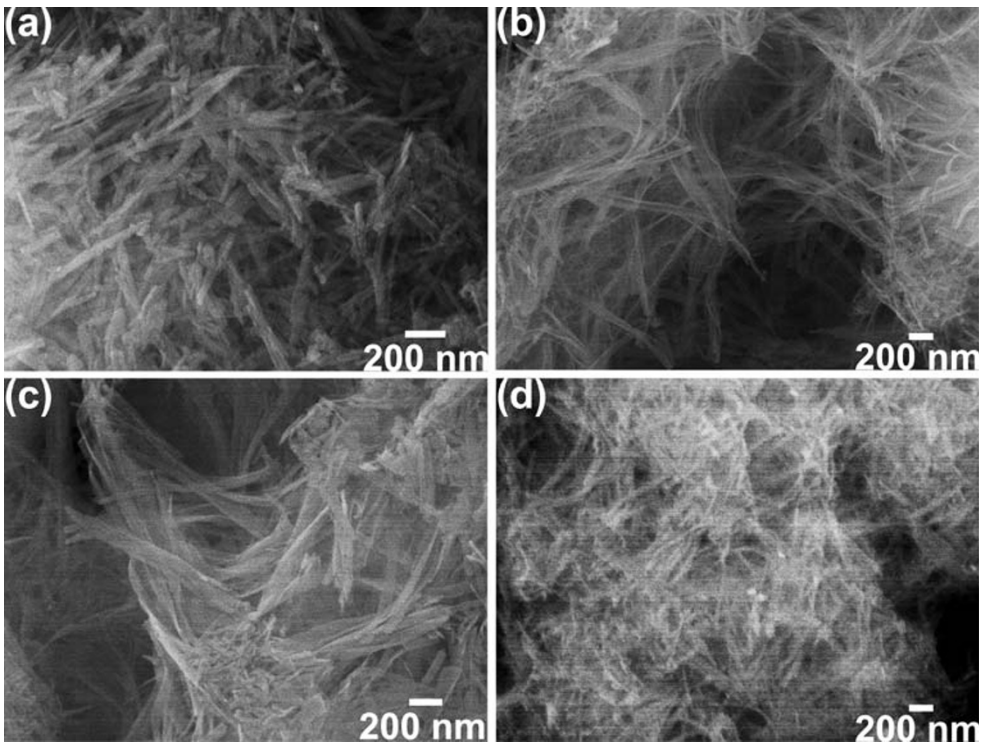

Fig. 7 SEM images of the MBH nanowhiskers annealed at 500 °C for 4 h. **a** MBH-NON, **b** MBH-CTAB, **c** MBH-SDS and **d** MBH-Triton

compared with the as-prepared sample, hence confirming the enhanced aspect ratio. From the above results, it can be concluded that the annealing of MBH nanowhiskers at 500 °C for 4 h does not have any significant effect on the crystalline phase of the MBH samples, but it does show slight change in the crystalline structure (Fig. 6) and prominent contribution toward the surface morphology as revealed in Fig. 7. The change in the surface morphology can arise due to the thermal elongation/contraction given to the fact that the as-synthesized MBH samples are partly amorphous in nature and thermal sensitive. Zhu et al. [8] also reported the increased aspect ratio of MBH nanowhiskers with annealing at controlled temperature, duration and heating rate.

UV–Vis Absorption and Photoluminescence

UV–vis absorption spectra of the MBH nanowhiskers synthesized with and without surfactants are recorded in the wavelength range of 250–800 nm at room temperature. Figure 8a presents the UV–vis spectra for as-synthesized MBH-NON nanowhiskers showing strong absorption in the low-wavelength (UV) region which can be attributed to the band gap absorption [34]. Optical band gap energy (Inset of Fig. 8a) is determined from the UV–vis absorption spectrum by plotting $(\alpha h\gamma)^2$ vs. photon energy, where α is the absorption coefficient, h is the Planck's constant and γ is the frequency of light [35]. The linear relation observed for $(\alpha h\gamma)^2$ vs. $h\gamma$ plot at high energy region (>4.5 eV) suggests that the MBH nanostructures are direct band gap materials. The intercept of the optical band edge curve on the energy axis (Inset of Fig. 8a) gives the optical band gap of about 4.15 eV [34]. The long tail of the absorption spectrum observed in the long wavelength region can exist due to the scattered radiation of the MBH nanostructures.

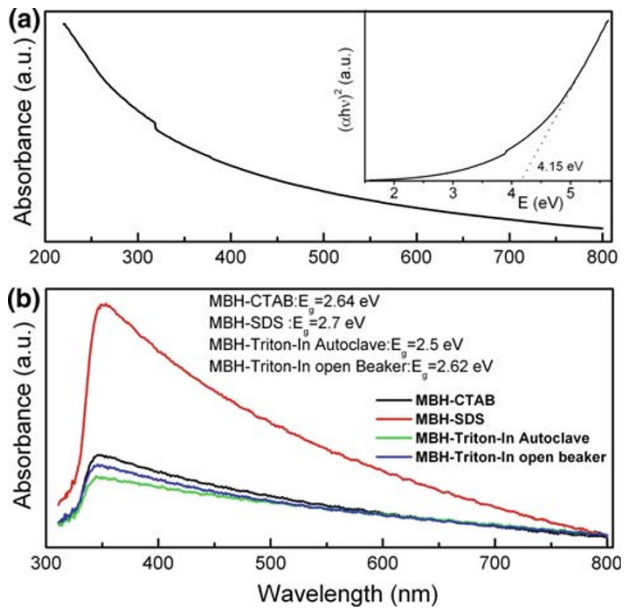

Fig. 8 UV–vis absorption spectra of the MBH nanowhiskers synthesized with and without surfactants. **a** Optical absorption spectrum of MBH-NON nanowhiskers; *inset* is the $(\alpha h\gamma)^2$ vs. $h\gamma$ plot with estimated optical band gap of about 4.15 eV, **b** Absorption spectra of MBH nanowhiskers synthesized with various surfactants; *inset* is the estimated optical band gaps determined from the optical band edge plots (not shown)

UV–vis absorption spectra of the as-synthesized MBH nanowhiskers formed with the assistance of surfactants are shown in Fig. 8b. When compared with the MBH-NON nanowhiskers, the nanostructures synthesized with surfactants show optical absorption peaks with maximum intensity at around 350 nm (photon energy of 3.55 eV), which can be related to the absorption in the band gap region. The optical band gap values estimated from the optical band edge plots ($(\alpha h\gamma)^2$ vs. $h\gamma$, not shown) for MBH-CTAB, MBH-SDS, MBH-Triton-In Autoclave and MBH-Triton-In open beaker are 2.64, 2.7, 2.5 and 2.62 eV, respectively. The large difference in the optical band gap for MBH-NON nanowhiskers and MBH nanowhiskers synthesized with various surfactants arises due to the fact that the surfactants can induce the formation of intermediate surface defect states in the band gap region [36]. The reduced optical band gap values can also be assigned to the increased aspect ratio of the nanowhiskers with the addition of surfactants (MBH-CTAB and MBH-Triton). The increase in the absorption peak intensity and band gap for MBH-SDS nanowhiskers in comparison with the MBH-CTAB and MBH-Triton-In Autoclave can be assigned to the reduced particle size [37]. MBH-Triton-In open beaker urchin-like nanowhiskers also shows increased band gap than the MBH-Triton-In Autoclave nanowhiskers due to the smaller particle size.

Photoluminescence measurement is a prominent tool for determining the crystalline quality of a material as well as its exciton fine structures. The PL properties of a material are characterized with both intrinsic and extrinsic effects, which usually give rise to discrete electronic states in the band gap region and will influence the emission processes [38]. In general, the PL emission of metal oxides is characterized by two bands: near-band-edge (NBE) ultraviolet emission and a deep level (DL) defect-related visible emission. The UV luminescence is commonly attributed to the direct recombination of excitons through an exciton–exciton scattering [39]. The visible luminescence originates from the radiative recombination of a photo-generated hole with an electron occupying the oxygen vacancy [40]. Figure 9 shows the room temperature PL spectra of the as-prepared MBH nanowhiskers at 200 °C for 24 h with and without surfactants, obtained in the wavelength range of 330–570 nm. The PL spectra of all MBH nanowhisker samples show a broad emission band covering the large

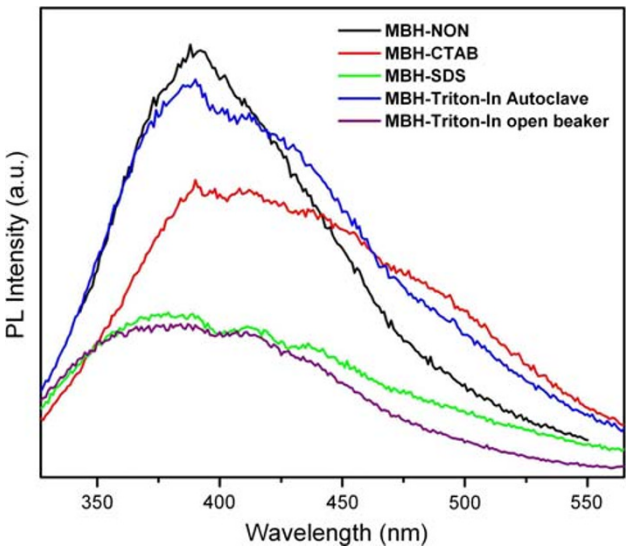

Fig. 9 Photoluminescence spectra of the as-synthesized magnesium borate hydroxide nanowhiskers formed with and without surfactants

wavelength range of 330–570 nm. The MBH-NON spectrum is centered at around 392 nm and is sharper than the PL spectra of MBH nanowhiskers synthesized with surfactants which show much broader band. The violet emission band at around 400 nm in the near UV region arises due to the direct transitions involving the valence band and conduction band in the band gap region. The PL spectra for MBH nanowhiskers synthesized with various kinds of surfactants show much broader features toward the visible region. In general, the overall shape of the visible emission depends on the defects, which in turn vary from sample to sample given their size and shape [41]. The peak broadening and peak position depend on the characteristics of the particles involved in the optical process, and the disparity in the peak position can be attributed to the same [42]. The luminescence in the visible region is usually related to various intrinsic or native defect centers and also the extrinsic defect/impurity centers formed during the preparation and also post-treatment, whereas these defects are normally located at the surface of the nanostructures given to their high surface area [36, 43]. The broad visible emission can also be attributed to the poor crystalline quality of the as-prepared MBH nanowhiskers, which is also confirmed from the XRD and TEM analysis. Indeed, the emission band is not distinctly distinguishable as NBE UV luminescence and DL visible emission. The broad emission band includes luminescence due to free excitons and defect or trapped states [39, 40]. However, the chemical origin of the defect related visible luminescence still remains controversial. The absence of expected strong NBE emission from these nanostructures implies that the surfaces of such particles are not completely passivated, leading to the presence of the surface states. Previous work by Liu et al. [26] demonstrated that Eu^{3+} doped single-crystal Szaibelyite $MgBO_2(OH)$ nanobelts show dominant red emission around 615 nm with excitation wavelength of 260 nm, which is visible to the naked eye, hence projecting $MgBO_2(OH)$ as a new host material for red-emitting rare-earth ions.

Conclusions

Magnesium borate hydroxide nanowhiskers of various shape and size were synthesized by hydrothermal route with and without using surfactants. The crystal structure and surface morphology of the MBH nanowhiskers are studied. XRD patterns reveal that the as-prepared nanowhiskers are pure $MgBO_2(OH)$ with monoclinic phase. The MBH samples synthesized with surfactants formed nanowhiskers with improved aspect ratio. The present synthesis technique produces $MgBO_2(OH)$ nanowhiskers with controlled shape and size at relatively low temperatures. The thermal annealing shows significant influence on the crystal structure and surface morphology of the MBH nanowhiskers. The MBH nanowhiskers synthesized with surfactants show reduced optical band gap (2.5–2.7 eV) than the MBH-NON sample (4.15 eV), which can be attributed to the increased aspect ratio and presence of surface defects with the addition of surfactants. The room temperature PL spectra of the MBH nanowhiskers synthesized with and without using surfactants show broad luminescence band at around 400 nm, which can be attributed to the violet emission originating from the surface defect states.

Acknowledgments This work was supported by the National Science Foundation under grant DMR-0548061. We would like to thank Dr. Dezhi Wang for his help with the TEM characterization.

References

1. A.P. Alivisatos, Science **271**, 933 (1996)
2. L. Lu, M.L. Sui, K. Lu, Science **287**, 1463 (2000)
3. Y. Cui, C.M. Lieber, Science **291**, 851 (2001)
4. G. Fasol, Science **280**, 545 (1998)
5. L.M. Peng, S.J. Zhu, Z.Y. Ma, J. Mi, F.G. Wang, H.R. Chen, D.O. Northwood, Mater. Sci. Eng. A **265**, 63 (1999)
6. Y. Takeuchi, Y. Kudoh, Am. Mineral. **60**, 273 (1975)
7. F.C. Hawthorne, Can. Mineral. **24**, 625 (1986)
8. W. Zhu, L. Xiang, Q. Zhang, X. Zhang, L. Hu, S. Zhu, J. Cryst. Growth **310**, 4262 (2008)
9. D.I. Shahare, S.J. Dhoble, S.V. Moharil, J. Mater. Sci. Lett. **12**, 1873 (1993)
10. Z.S. Hu, R. Lai, F. Lou, L.G. Wang, Z.L. Chen, G.X. Chen, J.X. Dong, Wear **252**, 370 (2002)
11. Y. Kashiwada, Y. Furuhata, Phys Status Solidi (A) **36**, K29 (1976)

12. H. Wang, G. Jia, Y. Wang, Z. You, J. Li, Z. Zhu, F. Yang, Y. Wei, C. Tu, Opt. Mater. **29**, 1635 (2007)
13. C. Furetta, G. Kitis, P.S. Weng, T.C. Chu, Nucl. Instrum. Methods Phys. Res. A **420**, 441 (1999)
14. E.M. Elssfah, H.A. Elsanousi, J. Zhang, H.S. Song, C. Tang, Mater. Lett. **61**, 4358 (2007)
15. R. Ma, Y. Bando, T. Sato, Appl. Phys. Lett. **81**, 3467 (2002)
16. Y. Li, Z. Fan, J.G. Lu, R.P.H. Chang, Chem. Mater. **16**, 2512 (2004)
17. J. Zhang, Z.Q. Li, B. Zhang, Mater. Chem. Phys. **98**, 195 (2006)
18. R. Ma, Y. Bando, D. Golberg, T. Sato, Angew. Chem. Int. Ed. **42**, 1836 (2003)
19. V. Russier, M.P. Pileni, Surf. Sci. **425**, 313 (1999)
20. S. Link, M.A. El-Sayed, J. Phys. Chem. B **103**, 8410 (1999)
21. J.M. Petroski, Z.L. Wang, T.C. Green, M.A. El-Sayed, J. Phys. Chem. B **102**, 3316 (1998)
22. H.S. Song, E.M. Elssfah, J. Zhang, J. Lin, J.J. Luo, S.J. Liu, Y. Huang, X.X. Ding, J.M. Gao, S.R. Qi, C. Cheng, J. Phys. Chem. B **110**, 5966 (2006)
23. S. Shi, M. Cao, X. He, H. Xie, Cryst. Growth Des. **7**, 1893 (2007)
24. W. Zhu, L. Xiang, T. He, S. Zhu, Chem. Lett. **35**, 1158 (2006)
25. W. Zhu, X. Zhang, L. Xiang, S. Zhu, Nanoscale Res. Lett. **4**, 724 (2009)
26. J. Liu, Y. Li, X. Huang, Z. Li, G. Li, H. Zeng, Chem. Mater. **20**, 250 (2008)
27. B.S. Xu, T.B. Li, Y. Zhang, Z.X. Zhang, X.G. Liu, J.F. Zhao, Cryst. Growth Des. **8**, 1218 (2008)
28. X. Teng, H. Yang, J. Mater. Chem. **14**, 774 (2004)
29. A.D.W. Carswell, E.A. O'Rear, B.P. Grady, J. Am. Chem. Soc. **125**, 14793 (2003)
30. D. Kuang, A. Xu, Y. Fang, H. Liu, C. Frommen, D. Fenske, Adv. Mater. **15**, 1747 (2003)
31. S. Santra, R. Tapec, N. Theodoropoulou, J. Dobson, A. Hebard, W. Tan, Langmuir **17**, 2900 (2001)
32. J. Israelachvili, D.J. Mitchell, B.W. Ninham, J. Chem. Soc., Faraday Trans. II **72**, 1525 (1976)
33. T. Ungár, Scr. Mater. **51**, 777 (2004)
34. A.F. Qasrawi, T.S. Kayed, A. Mergen, M. Gürü, Mater. Res. Bull. **40**, 583 (2005)
35. J.I. Pankove, *Optical Processes in Semiconductors* (Prentice Hall, New Jersey, 1971)
36. N.E. Hsu, W.K. Hung, Y.F. Chen, J. Appl. Phys. **96**, 4671 (2004)
37. U. Koch, A. Fojtik, H. Weller, A. Henglein, Chem. Phys. Lett. **122**, 507 (1985)
38. W. Shan, W. Walukiewicz, J.W. Ager III, K.M. Yu, H.B. Yuan, H.P. Xin, G. Cantwell, J.J. Song, Appl. Phys. Lett. **86**, 191911 (2005)
39. A.B. Djurišić, Y.H. Leung, Small **2**, 944 (2006)
40. K. Vanheusden, W.L. Warren, C.H. Seager, D.R. Tallant, J.A. Voigt, B.E. Gnade, J. Appl. Phys. **79**, 7983 (1996)
41. B. Cheng, W. Shi, J.M. Russell-Tanner, L. Zhang, E.T. Samulski, Inorg. Chem. **45**, 1208 (2006)
42. S. Ramanathan, S. Patibandla, S. Bandyopadhyay, J.D. Edwards, J. Anderson, J. Mater. Sci.: Mater. Electron **17**, 651 (2006)
43. D. Li, Y.H. Leung, A.B. Djurisic, Z.T. Liu, M.H. Xie, S.L. Shi, S.J. Xu, W.K. Chan, Appl. Phys. Lett. **85**, 1601 (2004)